7-20-2018

Effects of B and C doping on tunneling magnetoresistance in CoFe/MgO magnetic tunnel junctions

Andy Paul Chen
National University of Singapore

John D. Burton
University of Nebraska - Lincoln

Evgeny Y. Tsymbal
University of Nebraska-Lincoln, tsymbal@unl.edu

Yuan Ping Feng
National University of Singapore

Jingsheng Chen
National University of Singapore

Effects of B and C doping on tunneling magnetoresistance in CoFe/MgO magnetic tunnel junctions

Andy Paul Chen,[1] J. D. Burton,[2] Evgeny Y. Tsymbal,[2] Yuan Ping Feng,[1,3] and Jingsheng Chen[1,4]
[1]*NUS Graduate School of Integrative Sciences and Engineering, National University of Singapore, Singapore 117456, Singapore*
[2]*Department of Physics and Astronomy, University of Nebraska, Lincoln, Nebraska 68588-0299, USA*
[3]*Department of Physics, National University of Singapore, Singapore 117576, Singapore*
[4]*Department of Materials Science and Engineering, National University of Singapore, Singapore 117576, Singapore*

(Received 18 July 2017; revised manuscript received 11 May 2018; published 20 July 2018)

Using density-functional theory calculations, we investigate the dominant defects formed by boron (B) and carbon (C) impurities in a CoFe/MgO/CoFe magnetic tunnel junction (MTJ) and their influence on conductivity and tunneling magnetoresistance (TMR). We find that, in the O-poor conditions relevant to experiment, B forms the substitutional defect B_{Co} and C forms the interstitial site C_i at the CoFe/MgO interface. The C-doped MTJ is predicted to have a significantly higher TMR than the B-doped MTJ. This is due to interface state densities associated with the majority spin Δ_1-symmetry bands being more heavily suppressed by the B_{Co} defects than by the C_i defects. Our results indicate that carbon can serve as a viable alternative to boron as a dopant for MTJ fabrication.

DOI: 10.1103/PhysRevB.98.045129

I. INTRODUCTION

Magnetic tunnel junctions (MTJs) are devices comprising two ferromagnetic electrodes separated by a thin insulating barrier. The key functional property of an MTJ is tunneling magnetoresistance (TMR), which is the difference in MTJ resistance when the magnetizations of the two electrodes are aligned parallel or antiparallel [1]. The recent years have seen continuous development of MTJs to enhance the TMR, which is beneficial for applications. In particular, the use of MgO as an MTJ barrier material has come into focus, inspired by the theoretical predictions [2–5] and realized in experiment [6–8], making the CoFe/MgO/CoFe MTJ an attractive candidate for applications including magnetic random access memory devices and magnetic field sensors. It has been demonstrated that MgO-based MTJs exhibit TMR ratios up to 1100% at low temperatures [7] and 600% at room temperature [6], orders of magnitude higher than earlier iterations of MTJ using Ge [9] or amorphous Al-O_x barriers [10,11]. This is because the MgO barrier acts as a spin filter supporting transmission of majority-spin electrons of the Δ_1-symmetry state, which can be controlled by switching between parallel and antiparallel magnetization states, giving rise to the large TMR effect [2,12]. In CoFe/MgO/CoFe MTJs, this requires a coherent epitaxy between the Co/Fe (001) and MgO (001) layers, so that the metal atoms sit on top of the O atoms at the interface [13]. Industrial-scale fabrication of MTJs requires homogeneous thin-film growth over large surface areas via magnetron sputtering, so that atomically flat layers on the length scale of individual MTJ devices ($\sim$100 nm) can be achieved. It has been found that CoFeB is superior to CoFe in forming smooth, amorphous layers on MgO [8,14]. By annealing the films at 400 °C, this amorphous alloy crystallizes into a bcc structure epitaxial to the MgO (001) surface, using MgO as a crystallization template [14]. This process has allowed achieving greatly enhanced TMR [6,8], and the method has become widely adopted [15].

Despite its helpful role in fabrication, the presence of boron (B) atoms in the MTJ can create problems in device performance. First-principles calculations [16,17] have predicted that B atoms in CoFeB diffuse to the CoFe/MgO interface during the annealing process, and experimental observations using x-ray photoelectron spectroscopy (XPS) [18–20] have suggested that B atoms form oxide compounds at the CoFe/MgO interface. It has been predicted that the presence of B at the CoFe/MgO interface at interstitial sites of the CoFe layer suppresses the Δ_1-symmetry majority-spin conduction channels, leading to the reduction of TMR [16]. It has also been proposed that the formation of kotoite ($Mg_3B_2O_6$) at the CoFe/MgO interface is a factor reducing TMR [17]. The diffusion of B to the CoFe/MgO interface can be mitigated by a tantalum (Ta) layer, adjacent to CoFeB, into which B atoms diffuse preferentially [6,21–25]. However, Ta is prone to diffuse into the adjacent CoFe at high annealing temperatures, negatively affecting TMR [6].

In this study, using density-functional theory (DFT) calculations, we consider carbon (C) as an alternative dopant to B in fabricating a CoFe/MgO MTJ, due to the comparable atomic radii of B and C atoms. CoFeC alloys can exhibit colossal magnetocrystalline anisotropy [26] and retain a good epitaxy with the MgO layer [27]. However, the behavior of the C dopant in the annealing process of CoFe/MgO/CoFe MTJ fabrication and its impact on device TMR are less known. Therefore it would be interesting to identify the energetically favorable defect states in a CoFeC/MgO/CoFeC MTJ and study their effect on TMR.

II. DEFECT FORMATION

First, we analyze the defect formation energy as a measure of the thermodynamic stability and therefore the likelihood

of occurrence of a defect in the material. Using a supercell approach, we perform total-energy calculations to obtain the formation energy E^f of neutral B or C defect at the CoFe/MgO interface, which is given by [25,28]

$$E^f = E^t_{\text{defect}} - E^t_{\text{ideal}} + \sum_i \Delta N_i \mu_i. \quad (1)$$

Here, E^t_{defect} is the total energy of the supercell containing the defect, E^t_{ideal} is the total energy of the corresponding defect-free supercell, ΔN_i is the change in the number of atoms of species i made by introducing a defect to the supercell, and μ_i is the chemical potential of the atomic species. For μ_B, μ_C, μ_{Fe}, and μ_{Co}, we use the chemical potentials of the respective atoms in α-rhombohedral B, graphite, bcc Fe, and hcp Co, respectively. We consider the upper and lower bounds of μ_O as the total energy of one half of a free O_2 molecule (O-rich limit) and the chemical potential of O as MgO is reduced to hcp Mg (O-poor limit), respectively. μ_{Mg} is determined by the thermal equilibrium condition $\mu_{Mg} + \mu_O = E^t_{MgO}$ [29], where E^t_{MgO} is the energy of a two-atom unit of bulk MgO. We use a supercell of $4 \times 4 \times 4$ bcc CoFe unit cells and a supercell of $2 \times 2 \times 2$ MgO unit cells for defects in the interior of the CoFe and MgO layers, respectively. For defect formation at the CoFe/MgO interface, we use a supercell consisting of 11 (001) plane layers (2.7 nm) of CoFe and 5 (001) plane layers (1.1 nm) of MgO, corresponding to the lower bound of metal and barrier film thicknesses used in earlier experiments [6,30]. The ordered B2 phase is assumed for the CoFe layers and the energetically favored Co-terminated CoFe/MgO interface [16] is considered. The [100] direction of the CoFe is aligned with the MgO [110] direction at the interface so that the Co atoms at the interface are located directly above the O atoms in the MgO. The Co-O bond-length across the interface in the optimized structure is 2.16 Å. The in-plane lattice parameter of the supercell is constrained to 2.84 Å, corresponding to the lattice parameter of bulk CoFe. As a result, the MgO is strained compressively in-plane by 5.2% and undergoes a volume-conserving tetragonal distortion of about 4%. We consider interstitial and substitutional (replacing a Co, Fe, Mg, or O atom) defects in MgO, CoFe, or at the interface or subinterface atomic layers.

Structural relaxation and total energy calculations are performed using the pseudopotential plane-wave method with the generalized gradient approximation (GGA) [31] for the exchange-correlation energy implemented in the Vienna *ab initio* simulation package (VASP) [32,33]. A plane-wave basis set with a kinetic energy cutoff of 500 eV is used to expand the Kohn-Sham orbitals. For the reciprocal space sampling, a Monkhorst-Pack mesh is chosen to maintain a k-point spacing under 0.04 Å^{-1}. The Methfessel-Paxton method is used to treat partial occupancies with a smearing width of 0.2 eV. The E^f of each defect is then calculated from the total energy results.

Figure 1 summarizes the results of our computations. For all types of defects, we find that the defect formation energy decreases as the defect approaches the CoFe/MgO interface, indicating that both B and C would tend to diffuse to the interface region upon annealing. For B, this result is similar to earlier predictions [16,25]. In the oxygen rich (O-rich) condition, the most stable B defect is B_{Mg} at the MgO interface,

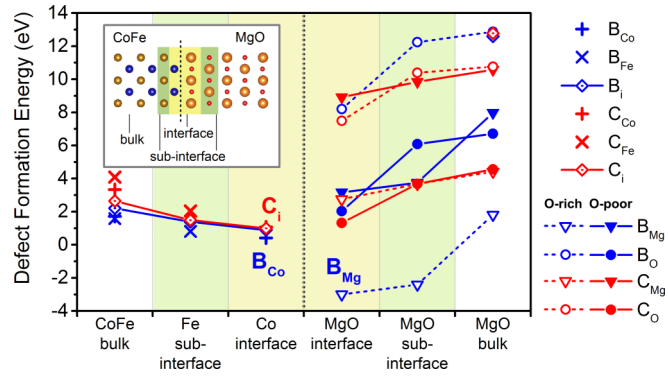

FIG. 1. Formation energies of defects created at different regions in the CoFe/MgO/CoFe MTJ (model of CoFe/MgO interface shown in inset). Defects with the lowest formation energies in (C_i, B_{Co}, and B_{Mg}) are labelled in the region where they occur in both O-rich and O-poor conditions.

where the B atom coordinates with four adjacent O atoms. In the oxygen poor (O-poor) condition, B tends to occupy the substitutional site at the interface Co layer (B_{Co}). At this site, the B-O distance across the interface is 3.0 Å, suggesting a weaker bonding compared to Co-O. C is predicted to create the interstitial defect C_i at the interface Co layer in both the O-rich and O-poor limits, owing to its comparatively small atomic radius. The defect causes a minor canting of Co-O bonds of approximately 2 degrees and a 0.15 Å ripple of the MgO interface atomic layer. We note that the O-poor condition corresponds more closely to the high-vacuum condition in rf magnetron sputtering, which is a common method for fabrication of the CoFeB/MgO/CoFeB MTJ [6,25,34].

III. EFFECTS ON TMR

Next, we study the effects of defects on TMR in CoFe/MgO/CoFe MTJs. We focus on the three types of defects, namely C_i, B_{Co}, and B_i, where the former two have the lowest formation energy in the O-poor condition corresponding to experiment, whereas the latter is used to help distinguish the effect of the dopant species from that of the defect site. The TMR ratio is defined as $(G^p - G^{ap})/G^{ap}$, where G^p and G^{ap} are, respectively, the conductance of the MTJ for parallel and antiparallel magnetization of the CoFe electrodes. The MTJ conductance is calculated using the Landauer-Büttiker formalism [35]. In this formalism, the spin-dependent tunneling conductance G_σ, for spin state $\sigma = \uparrow, \downarrow$, is proportional to the spin-dependent transmission probability $T_\sigma(\mathbf{k}_\parallel)$ summed up over all propagating states with in-plane wavevectors $\mathbf{k}_\parallel$. The total conductance G^s of a MTJ for a given device state s (parallel $s = p$ or antiparallel $s = ap$) is the sum of the spin-up and spin-down conductance:

$$G^s = G^s_\uparrow + G^s_\downarrow = \frac{e^2}{h} \sum_{\mathbf{k}_\parallel} T_\uparrow(\mathbf{k}_\parallel) + \frac{e^2}{h} \sum_{\mathbf{k}_\parallel} T_\downarrow(\mathbf{k}_\parallel) \quad (2)$$

In the transport calculations, the scattering region is defined by 5 atomic layers of MgO barrier between 6 atomic layers of bcc CoFe on each side. The dimensions of the supercell in the a and b directions are chosen to contain 2×2 in-plane unit cells

TABLE I. Tunneling conductivity (in $\Omega^{-1}m^{-2}$) of parallel-state ($\mathbf{G}^{p}_{\uparrow}$, $\mathbf{G}^{p}_{\downarrow}$) and antiparallel-state ($\mathbf{G}^{ap}$) magnetization of the electrodes for the defect-free CoFe/MgO/CoFe MTJ model and models containing $\mathbf{B_{Co}}$, $\mathbf{B_i}$, and $\mathbf{C_i}$.

Defect	$\mathbf{G}^{p}_{\uparrow}$	$\mathbf{G}^{p}_{\downarrow}$	$\mathbf{G}^{ap}$	TMR (%)
None	2.76×10^{11}	1.02×10^{11}	6.18×10^{9}	6020
$\mathbf{B_{Co}}$	6.00×10^{10}	7.92×10^{8}	7.77×10^{9}	682
$\mathbf{B_i}$	5.37×10^{11}	3.90×10^{9}	4.05×10^{10}	1240
$\mathbf{C_i}$	1.34×10^{12}	3.98×10^{9}	6.02×10^{10}	2130

of CoFe and 1 dopant atom per supercell, corresponding to a defect concentration of 3.1 atoms/nm^2, or a defect-defect distance of 5.68 Å. The left and right leads are bulk bcc CoFe. Electronic structure calculations are performed on the lead and scattering regions using the PW code implemented in Quantum ESPRESSO [36], using a kinetic energy cutoff of 500 eV and Monkhorst-Pack meshes with a spacing of under 0.02 Å^{-1}. The $\mathbf{k}_{\parallel}$-resolved transmission probabilities for majority-spin electrons ($T_{\uparrow}$) and minority-spin electrons ($T_{\downarrow}$) are then calculated using the PWCOND [37,38] code implemented in Quantum ESPRESSO.

Table I summarizes the calculated conductance of the individual spin channels ($G^{p}_{\uparrow}$, $G^{p}_{\downarrow}$, and G^{ap}) for a defect-free CoFe/MgO/CoFe MTJ and MTJs with the defects. For a defect-free MTJ, we find a very large TMR of 6020%, which is consistent with the earlier theoretical predictions [3,4]. This giant value of TMR is conventionally explained based on symmetry arguments, according to which a parallel-aligned MTJ exhibits much larger transmission than an antiparallel-aligned MTJ due to the Δ_1-symmetry majority-spin band in the CoFe electrodes matching the Δ_1-symmetry lowest decay evanescent state in MgO [2]. As is evident from Table I, the introduction of a defect reduces TMR. It is notable that the calculated TMR value for the B_{Co} defect is in agreement with the measured TMR values for CoFeB/MgO/CoFeB tunnel junctions at low temperature [6,34]. By comparing the calculated values of TMR for the two types of defects which have the lowest formation energy, i.e., C_i and B_{Co}, we see that C_i maintains a much higher TMR value (2130%) as compared to B_{Co} (682%), noting that the TMR for a MTJ with the C_i defect is also higher than that for a MTJ with the B_i defect. This is the central result of this work.

In the following, we explain the origin of this difference. We see from Table I that the majority-spin transmission dominated the total transmission for the parallel magnetization case and correlates with the TMR values for all the considered defect models. We therefore focus on the majority-spin transmission to understand the effect of particular defects on TMR. Figure 2(a) shows the $\mathbf{k}_{\parallel}$-resolved majority-spin transmission $T_{\uparrow}(\mathbf{k}_{\parallel})$ resolved in the 2D Brillouin zone for the different MTJ models. We find that the maximum $T_{\uparrow}$ occurs at $\mathbf{k}_{\parallel} = 0$, which is consistent with earlier analyses [3,12]. This is due to the dominant contribution from the Δ_1-symmetry band, which has the lowest decay rate in MgO. We see from Fig. 2(a) that the majority-spin transmission $T_{\uparrow}$ is reduced around $\mathbf{k}_{\parallel} = 0$ for the B_{Co} model but increased for the B_i and C_i models, as compared to the defect-free MTJ. In order to understand this difference, we calculate the $\mathbf{k}_{\parallel}$-resolved majority-spin

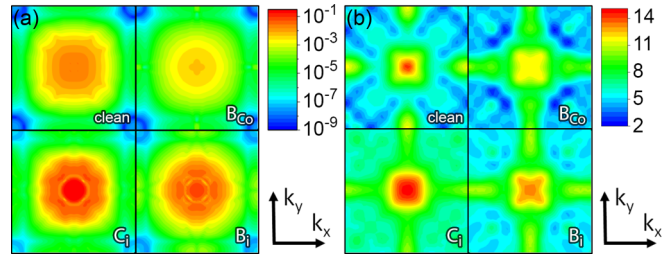

FIG. 2. (a) Majority-spin transmission probabilities $T_{\uparrow}$ and (b) $\mathbf{k}_{\parallel}$-resolved majority-spin density of states (in eV^{-1}) at the Fermi energy for the defect-free (clean) and defect-bearing (B_{Co}, B_i and C_i) CoFe/MgO/CoFe MTJs.

density of states (DOS) at the Fermi energy for each model. Figure 2(b) shows the result of this calculation for each model. We see that in all cases the dominant contribution to the majority-spin DOS originates from states close to the $\mathbf{k}_{\parallel} = 0$ point in the 2D Brillouin zone. Furthermore, we see that the magnitude of the majority-spin DOS at $\mathbf{k}_{\parallel} = 0$ correlates with the majority-spin transmission $T_{\uparrow}$. This result indicates that it is the majority-spin DOS which controls the effect of the defect state on TMR. Below, we elaborate this statement based on orbital symmetries.

IV. ORBITAL SYMMETRIES

The contributions of the different orbital symmetry states, defined at $\mathbf{k}_{\parallel} = 0$, to the transmission and TMR are studied by analyzing the density $|\psi|^2$ at the Fermi energy across the supercell [12,39]. For the parallel-aligned CoFe/MgO/CoFe MTJ, the majority-spin transmission is dominated by the Δ_1-symmetry band, while the minority-spin transmission is dominated the Δ_5-symmetry band. To illustrate the influence of different defects on spin transmission, we plot in Fig. 3 the state density of the majority-spin Δ_1 and minority-spin Δ_5 bands for each defect model. We observe that in all cases the minority-spin Δ_5 states decay fast into the interior of MgO and their densities are not changed significantly with the inclusion of B_{Co}, B_i, or C_i defects. On the contrary, the majority-spin Δ_1 states dominate the transmission and their densities are noticeably affected by the defect inclusion, with

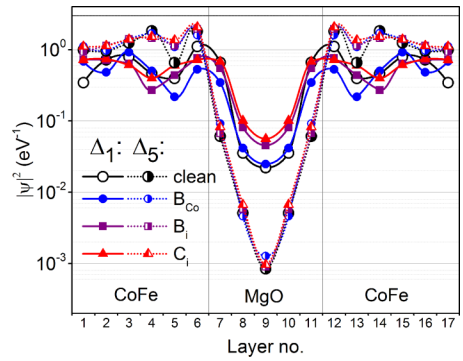

FIG. 3. State density $|\psi|^2$ for $\mathbf{k}_{\parallel} = 0$ majority-spin Δ_1 and minority-spin Δ_5 bands at the Fermi energy, projected on each atomic layer in the defect-free (clean) and defect-bearing (B_{Co}, B_i, and C_i) CoFe/MgO/CoFe MTJ.

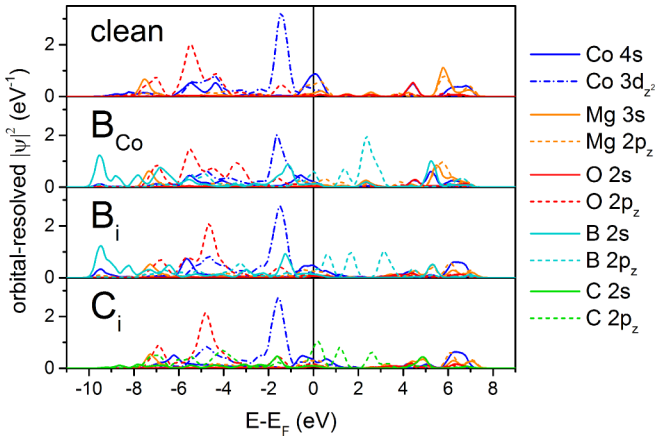

FIG. 4. Orbital-resolved state density $|\psi|^2$ of interface valence orbitals in defect-free (clean) and defect-bearing (B_{Co}, B_i, and C_i) CoFe/MgO/CoFe MTJ. The majority-spin state density at $\mathbf{k}_\parallel = 0$ is taken and orbitals associated with the Δ_1 symmetry (s, p_z, and d_{z^2}) are included.

B_{Co} suppressing the Δ_1 states at the CoFe/MgO interface more severely than B_i or C_i (layers number 6 and 7 in Fig. 3). This result shows that the stronger reduced majority-spin transmission and TMR for the B_{Co} defect in comparison to the B_i or C_i defects originate from the stronger suppression of the density of electronic states compatible to the Δ_1 symmetry at the CoFe/MgO interface.

The influence of defects on the majority-spin Δ_1 state density at $\mathbf{k}_\parallel = 0$ of individual valence orbitals at the interface is depicted in Fig. 4. Across all models, the interface hybridization between Co $3d_{z^2}$ and O $2p_z$ orbitals can be clearly seen. In the defect-free case, the peak in Co $4s$ state density at the Fermi energy is the dominant contributor to majority-spin Δ_1 state density at the interface. Introducing a defect diminishes the height of this peak, with B_{Co} diminishing it to a greater degree than B_i or C_i, due to the removal of an interface Co atom. Dopant $2p_z$ orbitals comprise a secondary contribution to interfacial majority-spin Δ_1 state density, with C $2p_z$ orbitals making the higher contribution.

V. SUMMARY

Based on the above analyses, we can summarize the results as follows. For epitaxial defect-free CoFe/MgO/CoFe MTJ, the bonding of Co and O atoms at the CoFe/MgO interface allows for a strong overlap between the Co $3d_{z^2}$ and O $2p_z$ orbitals (compatible with the Δ_1 symmetry), which mediates the efficient transmission of the majority-spin Δ_1 states, resulting in a high TMR. Introducing interstitial B or C atoms at the interface diminishes the state density of the interface Co $3d_{z^2}$ orbital at the Fermi energy. As a result, incident majority-spin electrons have lower transmission probability across the CoFe/MgO interface to enter the MgO layer, and thus the majority-spin transmission and TMR are reduced. A B_{Co} defect has an even stronger detrimental effect on TMR. Replacing a Co atom at the interface with B causes a larger suppression of the interface states compatible to the Δ_1 symmetry. This in turn leads to a stronger reduction of the majority-spin transmission, and hence the TMR.

In conclusion, using first-principles DFT calculations, we have explored the effect of B and C impurities in a CoFe/MgO/CoFe MTJ on the conductivity and TMR. By analyzing the defect formation energies of a variety of possible defects produced by B and C impurities, we have found that the favored defects are substitutional B_{Co} and interstitial C_i formed at the CoFe/MgO interface in the O-poor environment relevant to experiment. Based on electronic transport calculations, we have predicted that C_i is much more favorable to TMR in CoFe/MgO/CoFe MTJs than B_{Co}, due to a weaker suppression of the Δ_1-symmetry majority-spin density of states at the CoFe/MgO interface. Our results demonstrate that C can serve as a viable alternative to B as a dopant in MTJ fabrication.

ACKNOWLEDGMENTS

This work was completed utilizing the Holland Computing Center of the University of Nebraska-Lincoln and the National Supercomputing Centre (NSCC) Singapore. YPF and JSC acknowledge support from the Singapore National Research Foundation (NRF) under IIP Award No. NRF-IIP001-001. APC would like to thank Liu Xiaohui, Wu Qingyun, Ding-Fu Shao, and Lingling Tao for valuable discussions and advice.

[1] E. Y. Tsymbal, O. N. Mryasov, and P. R. LeClair, J. Phys. Condens. Matter **15**, R109 (2003).
[2] W. H. Butler, X. G. Zhang, T. C. Schulthess, and J. M. MacLaren, Phys. Rev. B **63**, 054416 (2001).
[3] J. Mathon and A. Umerski, Phys. Rev. B **63**, 220403 (2001).
[4] X. G. Zhang and W. H. Butler, Phys. Rev. B **70**, 172407 (2004).
[5] K. D. Belashchenko, J. Velev, and E. Y. Tsymbal, Phys. Rev. B **72**, 140404 (2005).
[6] S. Ikeda, J. Hayakawa, Y. Ashizawa, Y. M. Lee, K. Miura, H. Hasegawa, M. Tsunoda, F. Matsukura, and H. Ohno, Appl. Phys. Lett. **93**, 82508 (2008).
[7] S. Yuasa and D. D. Djayaprawira, J. Phys. D. Appl. Phys. **40**, R337 (2007).
[8] D. D. Djayaprawira, K. Tsunekawa, M. Nagai, H. Maehara, S. Yamagata, N. Watanabe, S. Yuasa, Y. Suzuki, and K. Ando, Appl. Phys. Lett. **86**, 092502 (2005).
[9] M. Jullière, Phys. Lett. A **54**, 225 (1975).
[10] J. S. Moodera, L. R. Kinder, T. M. Wong, and R. Meservey, Phys. Rev. Lett. **74**, 3273 (1995).
[11] T. Miyazaki and N. Tezuka, J. Magn. Magn. Mater. **139**, L231 (1995).
[12] W. H. Butler, Sci. Technol. Adv. Mater. **9**, 014106 (2008).
[13] J. F. Lawler, R. Schad, S. Jordan, and H. van Kempen, J. Magn. Magn. Mater. **165**, 224 (1997).
[14] S. Yuasa, Y. Suzuki, T. Katayama, and K. Ando, Appl. Phys. Lett. **87**, 242503 (2005).
[15] S. Ikeda, K. Miura, H. Yamamoto, K. Mizunuma, H. D. Gan, M. Endo, S. Kanai, J. Hayakawa, F. Matsukura, and H. Ohno, Nat. Mater. **9**, 721 (2010).
[16] J. D. Burton, S. S. Jaswal, E. Y. Tsymbal, O. N. Mryasov, and O. G. Heinonen, Appl. Phys. Lett. **89**, 142507 (2006).

[17] Z. Bai, L. Shen, Q. Wu, M. Zeng, J.-S. Wang, G. Han, and Y. P. Feng, Phys. Rev. B **87**, 014114 (2013).
[18] Y. Han, J. Han, H. J. Choi, H.-J. Shin, and J. Hong, Appl. Phys. Express **5**, 033001 (2012).
[19] Y. Han, J. Han, H. J. Choi, H.-J. Shin, and J. Hong, J. Mater. Chem. **21**, 14967 (2011).
[20] J. Y. Bae, W. C. Lim, H. J. Kim, T. D. Lee, K. W. Kim, and T. W. Kim, J. Appl. Phys. **99**, 08T316 (2006).
[21] X. Kozina, S. Ouardi, B. Balke, G. Stryganyuk, G. H. Fecher, C. Felser, S. Ikeda, H. Ohno, and E. Ikenaga, Appl. Phys. Lett. **96**, 072105 (2010).
[22] H. Kurt, K. Rode, K. Oguz, M. Boese, C. C. Faulkner, and J. M. D. Coey, Appl. Phys. Lett. **96**, 262501 (2010).
[23] A. A. Greer, A. X. Gray, S. Kanai, A. M. Kaiser, S. Ueda, Y. Yamashita, C. Bordel, G. Palsson, N. Maejima, S. H. Yang, G. Conti, K. Kobayashi, S. Ikeda, F. Matsukura, H. Ohno, C. M. Schneider, J. B. Kortright, F. Hellman, and C. S. Fadley, Appl. Phys. Lett. **101**, 202402 (2012).
[24] T. Hamada, T. Ohno, and S. Maekawa, Mol. Phys. **113**, 314 (2015).
[25] Z. Wang, M. Saito, K. P. McKenna, S. Fukami, H. Sato, S. Ikeda, H. Ohno, and Y. Ikuhara, Nano Lett. **16**, 1530 (2016).
[26] A. A. El-Gendy, M. Bertino, D. Clifford, M. Qian, S. N. Khanna, and E. E. Carpenter, Appl. Phys. Lett. **106**, 213109 (2015).
[27] C. Y. Chou, Y. D. Yao, P. C. Kuo, K. W. Cheng, C. Yu, and S. C. Chen, J. Magn. Magn. Mater. **310**, 2245 (2007).
[28] I. Tanaka, T. Mizoguchi, M. Matsui, S. Yoshioka, H. Adachi, T. Yamamoto, T. Okajima, M. Umesaki, W. Y. Ching, Y. Inoue, M. Mizuno, H. Araki, and Y. Shirai, Nat. Mater. **2**, 541 (2003).
[29] C. G. Van De Walle and J. Neugebauer, J. Appl. Phys. **95**, 3851 (2004).
[30] J. Hayakawa, S. Ikeda, F. Matsukura, H. Takahashi, and H. Ohno, Jpn. J. Appl. Phys. **44**, L587 (2005).
[31] Y. Wang and J. P. Perdew, Phys. Rev. B **44**, 13298 (1991).
[32] G. Kresse and J. Hafner, Phys. Rev. B **47**, 558 (1993).
[33] G. Kresse and J. Furthmüller, Comput. Mater. Sci. **6**, 15 (1996).
[34] Y. M. Lee, J. Hayakawa, S. Ikeda, F. Matsukura, and H. Ohno, Appl. Phys. Lett. **90**, 212507 (2007).
[35] H. D. Cornean, A. Jensen, and V. Moldoveanu, J. Math. Phys. **46**, 042106 (2005).
[36] G. Paolo, B. Stefano, B. Nicola, C. Matteo, C. Roberto, C. Carlo, C. Davide, L. C. Guido, C. Matteo, D. Ismaila, C. Andrea Dal, G. Stefano de, F. Stefano, F. Guido, G. Ralph, G. Uwe, G. Christos, K. Anton, L. Michele, M.-S. Layla, M. Nicola, M. Francesco, M. Riccardo, P. Stefano, P. Alfredo, P. Lorenzo, S. Carlo, S. Sandro, S. Gabriele, P. S. Ari, S. Alexander, U. Paolo, and M. W. Renata, J. Phys. Condens. Matter **21**, 395502 (2009).
[37] A. Smogunov, A. Dal Corso, and E. Tosatti, Phys. Rev. B **70**, 045417 (2004).
[38] H. J. Choi and J. Ihm, Phys. Rev. B **59**, 2267 (1999).
[39] W. H. Butler, X. G. Zhang, S. Vutukuri, M. Chshievand, and T. G. Schulthess, IEEE Trans. Magn. **41**, 2645 (2005).